Structural, Photoluminescence, and Field Emission Properties of Vertically Well-Aligned ZnO Nanorod Arrays

Chun Li,[†,‡] Guojia Fang,[*,†,‡] Nishuang Liu,[†] Jun Li,[†] Lei Liao,[†] Fuhai Su,[§] Guohua Li,[§] Xiaoguang Wu,[§] and Xingzhong Zhao[†]

Key Laboratory of Acoustic and Photonic Materials and Devices of the Ministry of Education, Department of Physics, Wuhan University, Wuhan, 430072, People's Republic of China, State Key Laboratory of Transducer Technology, Shanghai Institute of Microsystem and Information Technology, Chinese Academy of Sciences, Shanghai, 200050, People's Republic of China, and National Laboratory for Superlattices and Microstructures, Institute of Semiconductors, Chinese Academy of Sciences, Beijing, 100081, People's Republic of China

Received: May 16, 2007; In Final Form: June 27, 2007

The self-assembled growth of vertically well-aligned ZnO nanorod arrays with uniform length and diameter on Si substrate has been demonstrated via thermal evaporation and vapor-phase transport. The structural, photoluminescence (PL), and field emission properties of the as-prepared nanorod arrays were investigated. The PL spectrum at 10 K shows a strong and sharp near-band gap emission (NBE) peak (full width at half-maximum (FWHM) = 4.7 meV) and a weak neglectable deep-level emission (DL) peak (I_{NBE}/I_{DL}= 220), which implies its good crystallinity and high optical quality. The room-temperature NBE peak was deduced to the composition of free exciton and its first-order replicas emissions by temperature-dependent PL spectra. The field emission measurements indicate that, with a vacuum gap of 400 μm, the turn-on field and threshold field is as low as 2.3 and 4.2 V/μm. The field enhancement factor β and vacuum gap d follows a universal equation.

1. Introduction

One-dimensional (1D) nanostructural materials have attracted considerable attention due to their unique fundamental physical properties and potential high-technology applications in fabrication of nanoscale devices.[1] ZnO, which has a wide band gap of 3.37 eV, a large exciton binding energy of 60 meV at room temperature, and high mechanical and thermal stabilities,[2] is a promising semiconductor material for ultraviolet (UV) and blue optoelectronic devices. Vertically aligned ZnO nanowires have been extensively studied and demonstrated as chemical sensors,[3] field emitters,[4] and dye-sensitized solar cells.[5] Especially, lasing action has been observed on vertically aligned ZnO nanowires grown on the *a*-plane sapphire substrate due to efficient excitonic emission and natural resonance cavity structure of the nanowires.[6]

For the growth of vertically aligned ZnO nanowires, sapphire has been commonly used as substrates on which the growth is initiated, guided, and oriented by the catalyst particles. However, the presence of catalysts can not only be detrimental to the intrinsic physical properties of nanowires but also be harmful to their applications in nanodevices. Additionally, sapphire substrate is insulating, relatively expensive, and not compatible with semiconductor integrated techniques, which limited the applications of ZnO nanowires in photonic and electronic devices. Therefore, the catalyst-free growth of aligned ZnO nanowires on Si-based substrates has received increasing interest for their low-cost, large-scale production and is compatible with the well-developed Si-based semiconductor technology. Unfortunately, the large mismatches in the lattice constants and the thermal expansion coefficients would introduce a rather large residual strain between the ZnO nanowires and the Si substrate, resulting in the growth of poorly aligned ZnO nanowires. Recently, to reduce the lattice mismatch, a ZnO seed layer was deposited on Si substrate before the nanowire growth. Typically, well-aligned ZnO nanowire arrays can be obtained either by thermal evaporation or by hydrothermal methods.[7−11] Previously, using a highly *c*-oriented pulsed laser deposited (PLD) ZnO film as a seed layer, we reported the effect of substrate temperature on the synthesis of ZnO nanorods via vapor-phase transport.[8] In this work, we focused on the structural, photoluminescence (PL), and field emission properties of hexagonal-shaped, well-facetted and aligned, and high crystal quality and aspect-ratio ZnO nanorods with uniform diameter and length, which would pave the way toward a silicon-compatible vertical surface emitting laser and field emitter arrays for lighting and display applications.

2. Experimental Methods

ZnO nanorods were fabricated by using a simple thermal evaporation and vapor-phase transport in a horizontal tube furnace. The details of the nanorod synthesis process have been previously reported by our group.[8] Briefly, a 200 nm ZnO film was first deposited on a Si (100) substrate at a temperature of 500 °C with oxygen pressure of 0.02 Pa by PLD. After the film deposition, a powder mixture of ZnO (99.99%) and graphite (99.9%) with a molar ratio of 1:1 was placed in the closed end of a one-end-sealed small quartz tube. The ZnO-coated silicon substrates were placed definite distances away from the

* To whom correspondence should be addressed. Telephone: +86 27 87642784. Fax: +86 27 68752569. E-mail: gjfang@whu.edu.cn.
† Wuhan University.
‡ Shanghai Institute of Microsystem and Information Technology, Chinese Academy of Sciences.
§ Institute of Semiconductors, Chinese Academy of Sciences.

10.1021/jp0737808 CCC: $37.00
Published on Web 08/08/2007

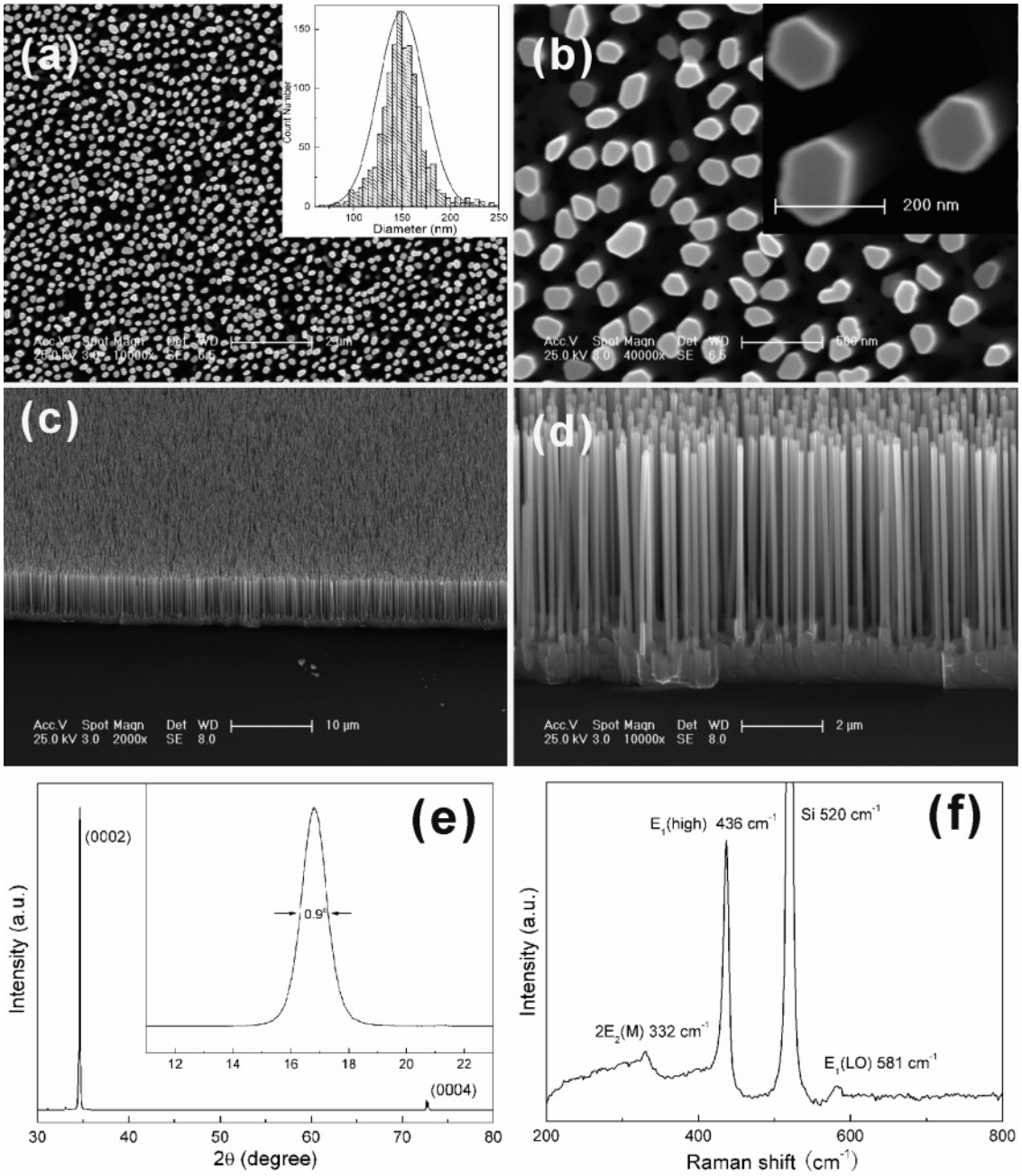

Figure 1. SEM images of vertically well-aligned ZnO nanorod arrays: (a, b) Top view; (c, d) 50° tilted view. The hexagonal cross-section morphologies can be clearly seen in inset of b. (e) XRD pattern and (f) Raman spectrum of ZnO nanorod arrays. The inset in e shows the θ-rocking curve of the (0002) peak. The inset in a shows the diameter distribution.

evaporation source in the small quartz tube. Then, the small tube was pushed into the tube furnace with the source positioned at the center of the furnace, while the open end was put against the gas flow direction. The furnace was heated at a rate of 25 °C/min and held at 950 °C for 8 min. The local temperature of the substrate was about 850 °C. During the whole synthesis process, a constant flow of 100 cm^3(STP) min^{-1} of Ar gas was introduced to the furnace and the pressure in the tube was kept at about 200 Pa. Finally, the substrates were naturally cooled to room temperature under Ar flow in the furnace.

The morphology and structure of products were characterized with field emission scanning electron microscopy (FE-SEM, Philips FEI XL30) and X-ray diffraction (XRD, D8 Advance, Cu Kα). Micro-Raman measurements were performed at room temperature by a Renishaw (RM1000) confocal micro-Raman spectrometer using the 514.5 nm Ar^+ laser as the excitation source. The PL spectra were obtained by using a He−Cd laser (325 nm) as excitation source from 10 to 293 K. The field emission characteristics of as-prepared nanorod arrays were investigated at room temperature in a vacuum chamber of 10^{-7} Pa. The sample was used as the cathode, and a molybdenum probe with 1 mm in diameter acted as the anode. The distance between the two electrodes was precisely adjusted by a micrometer. The emission current was measured using a Keithley 485 picoammeter.

3. Results and Discussion

A. Morphologies and Crystal Structure Characterization. Parts a−d of Figure 1 show the detailed morphologies of the as-prepared ZnO nanorods. A well-aligned nanorod array with high density was observed on the entire surface of the substrate. Almost every nanorod is perpendicularly to the substrate. The nanorods have a uniform length of about 8 μm. According to

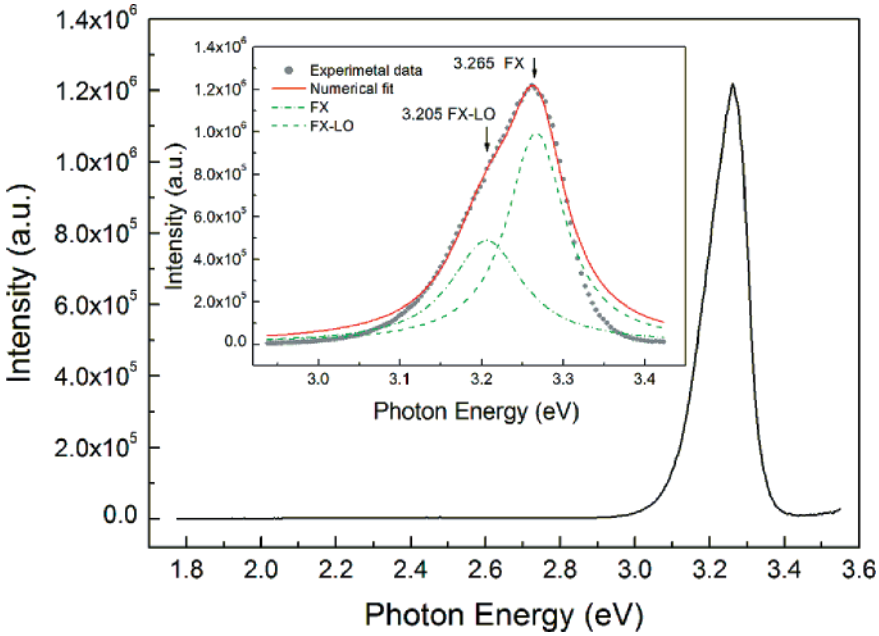

Figure 2. Room-temperature PL spectrum of ZnO nanorods. The inset shows the Lorentz fitting results of UV region with free exciton and its first-order phonon replicas.

the diameter histogram, as shown in the inset of Figure 1a, the diameters of the nanorods distribute in a narrow range of 100−200 nm and have an average value of 150 nm. The end planes of the nanorods are smooth hexagons that correspond to the (0001) crystal plane of ZnO, as shown in the inset of Figure 1b. Figure 1e shows the $\theta-2\theta$ XRD pattern from the as-prepared products, with the ZnO (0002) and (0004) peaks clearly observed at 34.56 and 72.66°, respectively. The full widths at half-maximum (FWHM) of the θ-rocking curve of the (0002) peak shown in the inset of Figure 1e is 0.9°, which is much lower than the values for nanorods reported in the literature,[7] demonstrating their excellent alignment.

Raman spectra are sensitive to crystallization, structural disorder, and defects in micro-/nanostructures. Therefore, the vibrational properties of as-prepared ZnO nanorods were investigated by Raman-scattering techniques at room temperature, as shown in Figure 1f. The appearance of a dominant, sharp, and strong peak at 438 cm^{-1} is attributed to the Raman active optical phonon E_2(high) mode of the ZnO, confirming that the as-prepared nanorods have the wurtzite hexagonal phase. The peak at 332 cm^{-1} is also observed, which can be attributed to the second-order Raman processes. The peak at 581 cm^{-1} is attributed to the E_1(LO) mode, which might be observed due to formation of defects such as zinc interstitials and oxygen vacancies.[11,12] Therefore, the sharp and dominant E_2(high) mode with weak E_1(LO) mode in the Raman spectrum indicates that the as-prepared ZnO nanorods are highly crystalline with less structural defects.

B. Photoluminescence Properties. Figure 2 shows room-temperature PL spectrum of ZnO nanorods, which exhibits a strong and sharp peak at 3.26 eV (380 nm) in the UV region with no other distinguished emission band in the visible region. Due to the average rod diameter of 150 nm, which is too large for quantum effects to be observed, the charge carriers in ZnO nanorods do not experience quantum confinement effects. Clearly, the UV emission peak shows an asymmetry shape. Despite many studies, the exact mechanisms of UV PL and carrier recombination processes in ZnO nanostructures are still the subjects of considerable debates. Various investigations arrived at different conclusions, and there is no agreement about the origin of UV PL in ZnO nanostructures.[13,14] Namely, UV PL was attributed to the confined excitons,[15] transverse optical phonon band of the confined excitons,[16,17] donor-bound excitons,[18,19] or acceptor-bound excitons.[20,21] To address the nature of the UV emission for our as-prepared samples, we have studied the temperature-dependent PL spectra.

The inset in Figure 3a shows the PL spectrum at 10 K; the emission bands are composed of a strong UV band around 3.366 eV (369 nm) and a very weaker green emission band around 2.4 eV (516 nm). The latter has been mainly suggested to the singly ionized oxygen vacancy in ZnO, although several different hypotheses have been proposed.[13] The FWHM of UV peaks is 4.7 meV, which is comparable to that observed in the ZnO single crystal.[22] The intensity ratio of the UV and green emission is 220, which is higher than that of high-quality ZnO epilayers prepared by molecular beam epitaxy, indicating their good crystallinity with excellent optical properties.[15,23] According to their energy values and separation (LO-phonon energy of ZnO, about 72 meV),[16] the excitonic features of the UV PL spectrum at 10 K were associated with free-exciton (FX), donor-bound exciton (D°X), LO-phonon replicas of FX, and LO-phonon replicas of D°X, as shown in Figure 3a. No surface-related exciton peaks were observed.[24] To see the detailed evolution of exciton peaks, the deconvolution of the PL spectrum in the range of 3.34−3.40 eV from 10 to 113 K by Lorentz curve fitting was carried out, as depicted in Figure 3b. Clearly, the emission band can be divided into three independent peaks (two D°X emissions for I_3 and I_1 lines[25] and one FX line). We found that I_3 and I_1 merged into a single D°X peak at 113 K, and their intensity decreases quickly with the increase of temperature. As the temperature continues increasing, the D°X peak gradually gets weaker and broadened and finally merges into the low-energy tail of the FX peak at the temperature above 143 K, which is due to the thermal ionization of bound excitons into free excitons at higher temperature for its smaller binding energy.[26] Meanwhile, FX-*n*LO peaks are more dominant than D°X-*n*LO peaks at 10 K and D°X-*n*LO peaks quickly disappear as temperature increases, which means LO-phonons have a stronger coupling interaction with FX than that with D°X. The FX and FX-*n*LO peaks become dominant above 53 K, and then

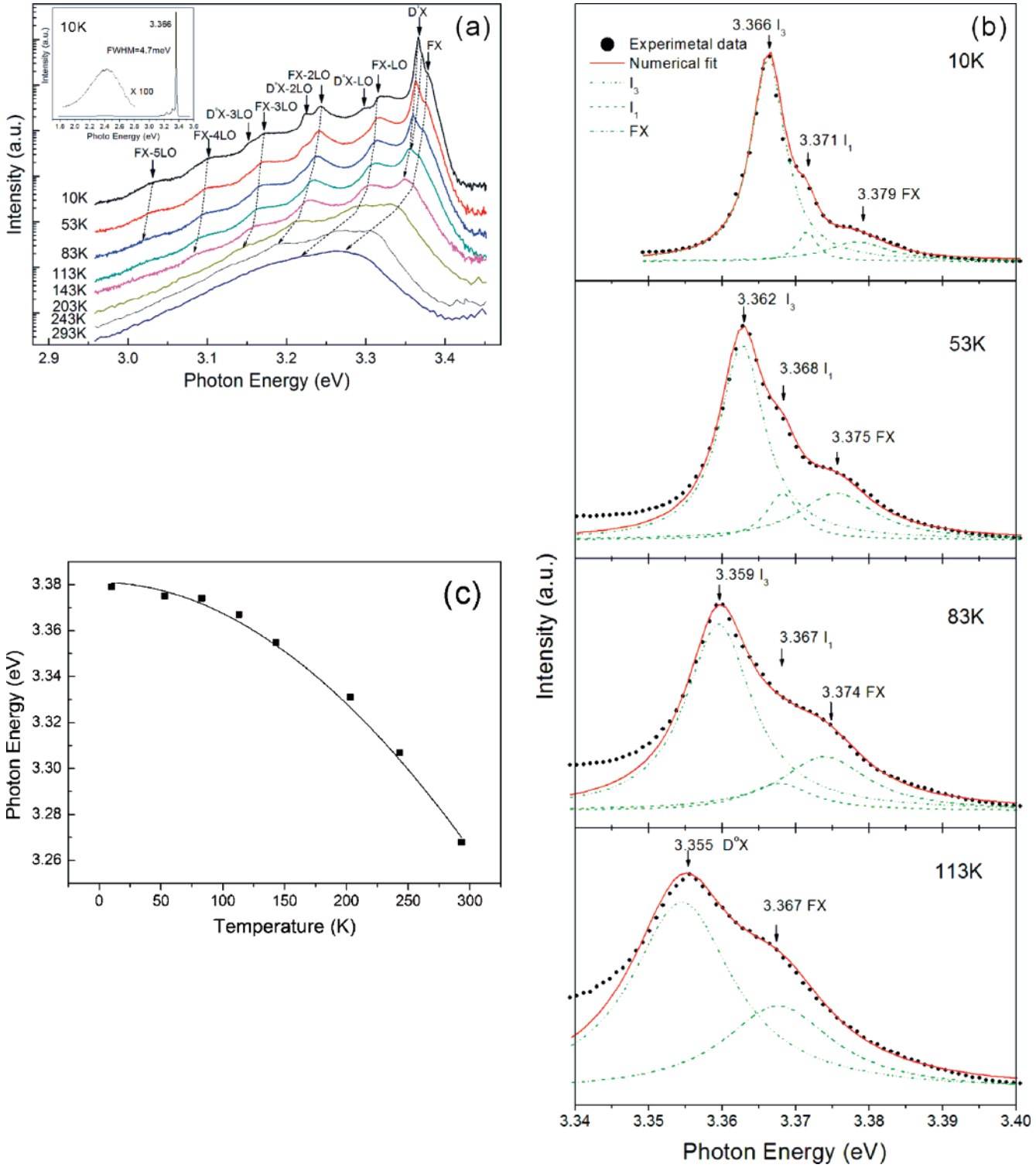

Figure 3. (a) PL spectra measured from 10 to 293 K. (b) Deconvolution of PL spectra by Lorentz fitting to show the detailed evolution from 10 to 113 K. (c) Peak energy of the FX as a function of temperature ranging from 10 to 293 K. The solid line is the theoretical fit to the experimental data (dots) by Varshni's formula.

the FX and FX-*n*LO emissions start to merge together due to the broader spectral shape at higher energy side of each FX-*n*LO emission. At room temperature, the FX and FX-1LO were found at 3.26 and 3.20 eV, respectively, which is consistent with the curve fitting results as shown in the inset of Figure 2. The slight variation in the energy separation between FX and its phonon replicas with temperature is related to the redistribution of excitons in the band (i.e., exciton thermalization) with increasing temperature.[24]

Figure 3c shows the temperature dependence of the FX peak positions. The red shift with increasing temperature supports its excitonic origin. Due to the temperature-induced change of lattice parameters and electron−lattice interaction, the free excitonic energy follows the well-known Varshni's empirical formula: $E(T) = E(0) - \alpha T^2/(T + \beta)$, where $E(0)$ is an exciton energy at $T = 0$ K and α and β are Varshni thermal coefficients.[21] The result of the fitting curve is shown as a solid line through the data points in Figure 3c, where the best values

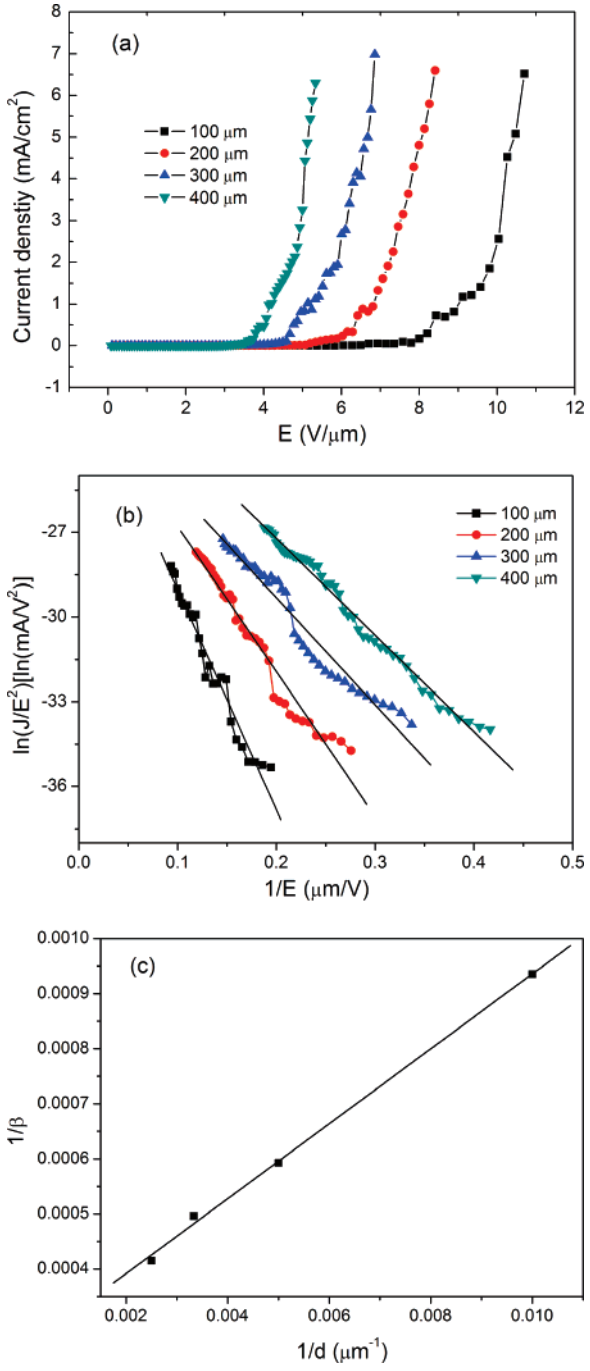

Figure 4. (a) Field emission current density as a function of electric field, (b) corresponding FN plots at different vacuum gaps, and (c) relationship of β and d. The straight line is the linear fit to experimental data (dots) based on the TRFE model.

of $E(0)$, α, and β are 3.381 eV, 0.00587 eV/K, and 4249 K, respectively. These fitting values are in reasonable agreement with the literature report for nanocrystalline ZnO thin films grown on Si substrates.[27]

C. Field Emission Properties. Recently, 1D nanomaterial such as carbon nanotubes (CNTs) and semiconductor nanowires has attracted much attention for their good field emission properties. It is well-known that CNTs generally show a low turn-on field of about 0.5−2 V/μm and a high-emission current density of about several mA/cm^2.[28−30] However, CNTs can be easily degraded in ambient oxygen even though they show good emission behavior. ZnO, as an oxide, exhibits strong endurance to ambient oxygen compared with CNTs.[31] Therefore, in this work, we tried to evaluate field emission properties of our as-prepared ZnO nanorods. Figure 4a illustrates the emission current density as a function of the electric field of ZnO nanorods measured at different vacuum gaps (d). The turn-on electric field (corresponding to the current density of 1 μA/cm^2) was about 5.1, 3.6, 2.7, and 2.3 V/μm at d = 100, 200, 300, and 400 μm, respectively. And the threshold field (corresponding to the current density of 1 mA/cm^2) was about 9.0, 6.9, 5.1, and 4.2 V/μm, respectively. The current density at 6.8 V/μm is as high as 7 mA/cm^2 at d = 200 μm, and no current saturation is observed. Lower turn-on field, lower threshold field, and higher current density of field emission have been obtained from our ZnO nanorod arrays, compared with those of the aligned ZnO nanowires reported in the literature, such as catalyst-free nanowires grown on Si substrate,[32] nanowires grown on Co catalyst particles,[33] and needlelike nanowires grown on a Ga-doped ZnO film.[9] For the nanorods fabricated by our approach, almost every single nanorod was grown perpendicularly to the Si substrate, which can be of great benefit to electron emission.

The $J-E$ characteristics were further analyzed by the Fowler−Nordheim (FN) plot using the FN equation, $\ln(J/E^2) = \ln(A\beta^2/\phi) - B\phi^{3/2}/\beta E$, where $A = 1.54 \times 10^{-6}$ A eV V^{-2}, $B = 6.83 \times 10^9$ eV$^{-3/2}$ V m^{-1}, β is the field enhancement factor, and ϕ is the work function of emitter materials, as shown in Figure 4b. β can be calculated from the slope of the fitting line of FN plots, $\ln(J/E^2)$ vs $1/E$. Considering that the work function of ZnO is 5.3 eV,[9] β is calculated to be 1069, 1686, 2014, and 2410 for d = 100, 200, 300, and 400 μm, respectively. For different nanostructures, β is strongly dependent on the morphologies and geometric configuration of emitters, such as curve radii, aspect ratio, alignment, and density of emitters. For certain emitters, β is also dependent on the geometry of the anode−cathode system, especially the vacuum gap d. Therefore, β is an important parameter in describing field emission, and the relationship between β and d is helpful for fabrication field-emission devices. Figure 4c is a relationship of $1/\beta$ vs $1/d$. On the basis of the two-region field-emission (TRFE) model,[34,35] we found that the experimental data are almost fitted to be a straight line and can be described by the equation $1/\beta = h/d + 1/\beta_0$, where h is the width of the field enhancement region near the nanorod surface and β_0 is the absolute amplification factor, which is intrinsically determined by emitters and independent of d and applied field. h and β_0 are about 66 nm and 3738. h is much smaller than the values in literature report (h is 540 nm for CNT grown on Si wafer[34]), which is probably due to the strong screening effect caused by the higher density of the nanorod arrays.

4. Conclusions

Vertically well-aligned ZnO nanorods with uniform length and diameter have been synthesized on silicon substrate by vapor-phase transport. Temperature-dependent PL spectra demonstrated the as-prepared ZnO nanorods have high crystal and optical qualities. The room-temperature NBE peak was deduced to the composition of free exciton and its first-order replica emissions by the evolution of temperature-dependent PL spectra and the fitting of Varshni's empirical formula. The field emission properties indicate the emission current density increases with the increase of the anode−cathode gap under the same applied field. The experimental data well agreed with FN theory and followed a universal equation between β and d. The nanorods exhibit good alignment and optical properties, which are very useful for many applications such as nanoscale ultraviolet laser diodes, UV optical detectors, and optical

switches. In addition, the emission current from ZnO nanowires synthesized on a Si substrate without the presence of a catalyst is sufficient for field emission displays and vacuum microelectronic devices.

Acknowledgment. This research was supported by the Natural Science Foundation of Hubei Province under Grant No. 2006ABA215 and by the Foundation of the State Key Laboratory of Transducer Technology, China.

References and Notes

(1) Xia, Y.; Yang, P.; Sun, Y.; Wu, Y.; Mayers, B.; Gates, B.; Yin, Y.; Kim, F.; Yan, Y. *Adv. Mater.* **2003**, *15*, 353.

(2) Özgür, Ü.; Alivov, Y. I.; Liu, C.; Teke, A.; Reshchikov, M. A.; Doğan, S.; Avrutin, V.; Cho, S. J.; Morkoç, H. *J. Appl. Phys.* **2005**, *98*, 041301.

(3) Zhang, Y. S.; Yu, K.; Jiang, D. S.; Zhu, Z. Q.; Geng, H. R.; Luo, L. Q. *Appl. Surf. Sci.* **2005**, *242*, 212.

(4) Banerjee, D.; Jo, S. H.; Ren, Z. F. *Adv. Mater.* **2004**, *16*, 2028.

(5) Law, M.; Greene, L. E.; Johnson, J. C.; Saykally, R.; Yang, P. D. *Nat. Mater.* **2005**, *4*, 455.

(6) Huang, M. H.; Mao, S.; Feick, H.; Yan, H. Q.; Wu, Y. Y.; Kind, H.; Weber, E.; Russo, R.; Yang, P. D. *Science* **2001**, *292*, 1897.

(7) Jie, J. S.; Wang, G. Z.; Chen, Y. M.; Han, X. H.; Wang, Q. T.; Xu, B.; Hou, J. G. *Appl. Phys. Lett.* **2005**, *86*, 031909.

(8) Li, C.; Fang, G. J.; Fu, Q.; Su, F. H.; Li, G. H.; Wu, X. G.; Zhao, X. Z. *J. Cryst. Growth* **2006**, *292*, 19. Li, C.; Fang, G. J.; Su, F. H.; Li, G. H.; Wu, X. G.; Zhao, X. Z. *Nanotechnology* **2006**, *17*, 3740.

(9) Tseng, Y. K.; Huang, C. J.; Cheng, H. M.; Lin, I. N.; Liu, K. S.; Chen, I. C. *Adv. Funct. Mater.* **2003**, *13*, 811.

(10) Choy, J. H.; Jang, E. S.; Won, J. H.; Chung, J. H.; Jang, D. J.; Kim, Y. W. *Adv. Mater.* **2003**, *15*, 1911.

(11) Chen, S. J.; Liu, Y. C.; Lu, Y. M.; Zhang, J. Y.; Shen, D. Z.; Fan, X. W. *J. Cryst. Growth* **2006**, *289*, 55.

(12) Xu, C. X.; Sun, X. W. *Jpn. J. Appl. Phys.* **2003**, *42*, 4949.

(13) Djurišić, A. B.; Leung, Y. H. *Small* **2006**, *2*, 944.

(14) Fonoberov, V. A.; Alim, K. A.; Alexander, B. A.; Xiu, F.; Liu, J. *Phys. Rev. B* **2006**, *73*, 165317.

(15) Mahamuni, S.; Borgohain, K.; Bendre, B.; Leppert, S. V. J.; Risbud, S. H. *J. Appl. Phys.* **1999**, *85*, 2861.

(16) Wong, E. M.; Searson, P. C. *Appl. Phys. Lett.* **1999**, *74*, 2939.

(17) Matsumoto, T.; Kato, H.; Miyamoto, K.; Sano, M.; Zhukov, E. A. *Appl. Phys. Lett.* **2002**, *81*, 1231.

(18) Liu, Y. L.; Liu, Y. C.; Feng, W.; Zhang, J. Y.; Lu, Y. M.; Shen, D. Z.; Fan, X. W.; Wang, D. J.; Zhao, Q. D. *J. Chem. Phys. B* **2005**, *122*, 174703.

(19) Najafov, H.; Fukada, Y.; Ohshio, S.; Iida, S.; Saitoh, H. *Jpn. J. Appl. Phys., Part 1* **2003**, *42*, 3490.

(20) Zhang, X. T.; Liu, Y. C.; Zhi, Z. Z.; Zhang, J. Y.; Lu, Y. M.; Shen, D. Z; Xu, W.; Fan, X. W.; Kong, X. G. *J. Lumin.* **2002**, *99*, 149.

(21) Chen, J.; Fujita, T. *Jpn. J. Appl. Phys., Part 2* **2002**, *41*, L203.

(22) Reynold, D. C.; Look, D. C.; Jogai, B.; Litton, C. W.; Harsch, W.; Cantwell, G. *Phys. Rev. B* **1998**, *57*, 12151.

(23) Bagnall, D. M.; Chen, Y. F.; Shen, M.Y.; Zhu, Z.; Goto, T.; Yao, T. *J. Cryst. Growth* **1998**, *184/185*, 605.

(24) Voss, T.; Bekeny, C.; Wischmeier, L.; Gafsi, H.; Bömer, S.; Schade, W.; Mofor, A. C.; Bakin, A.; Waag, A. *Appl. Phys. Lett.* **2006**, *89*, 182107.

(25) Meyer, B. K.; Alves, H.; Hofmann, D. M.; Kriegseis, W.; Forster, D.; Bertram, F.; Christen, J.; Hoffmann, A.; Strassburg, M.; Dworzak, M.; Haboeck, U.; Rodina, A. V. *Phys. Status Solidi B* **2004**, *241*, 231.

(26) Jung, S .W.; Park, W. I.; Cheong, H. D.; Yi, G. C.; Jang, H. M.; Hong, S.; Joo, T. *Appl. Phys. Lett.* **2002**, *80*, 1924.

(27) Zhang, Y.; Lin, B.; Sun, X.; Fu, Z. *Appl. Phys. Lett.* **2005**, *86*, 131910.

(28) Zhu, W.; Bower, C.; Zhou, O.; Kochanski, G.; Jin, S. *Appl. Phys. Lett.* **1999**, *75*, 873.

(29) Lee, C. J.; Park, J.; Kang, S. Y.; Lee, J. H. *Chem. Phys. Lett.* **2000**, *326*, 175.

(30) Bonard, J. M.; Weiss, N.; Kind, H.; Stokli, T.; Forro, L.; Kern, K.; Chatelain, A. *Adv. Mater.* **2001**, *13*, 184.

(31) Cheng, A.-J.; Wang, D.; Seo, H. W.; Liu, C.; Park, M.; Tzeng, Y. *Diamond Rel. Mater.* **2006**, *15*, 426.

(32) Ham, H.; Shen, G. Z.; Cho, J. H.; Lee, T. J.; Seo, S. H.; Lee, C. J. *Chem. Phys. Lett.* **2005**, *69*, 404.

(33) Lee, C. J.; Lee, T. J.; Lyu, S. C.; Zhang, Y.; Ruh, H.; Lee, H. J. *Appl. Phys. Lett.* **2002**, *81*, 3648.

(34) Zhong, D. Y.; Zhang, G. Y.; Liu, S.; Sakurai, T.; Wang, E. G. *Appl. Phys. Lett.* **2002**, *80*, 506.

(35) Xue, X. Y.; Li, L. M.; Yu, H. C.; Chen, Y. J.; Wang, Y. G.; Wang, T. H. *Appl. Phys. Lett.* **2006**, *89*, 043118.